Electronic Supplementary Material (ESI) for Dalton Transactions.

Supplementary Material

Helix-Coil Transition Induced by Metal-Ion Interaction with a Grafted Iron-Binding Site of the CyaY Protein Family

Diego S. Vazquez[a,‡], William A. Agudelo[a,‡], Angel Yone[a], Nora Vizioli[a], Martín Arán[b], F. Luis González Flecha[a], Mariano C. González Lebrero[a,*] and Javier Santos[a,*]

[a]Instituto de Química y Físico-Química Biológicas, Universidad de Buenos Aires - CONICET. Junín 956, 1113AAD, Buenos Aires, Argentina.

[b]Fundación Instituto Leloir and IIBBA-CONICET, Av. Patricias Argentinas 435, 1405 Buenos Aires, Argentina.

[*]Correspondence should be addressed to nanolebrero@gmail.com and javiersantosw@gmail.com

Tel: +54 11 49648290, ext. 108. Fax: +54 11 49625457

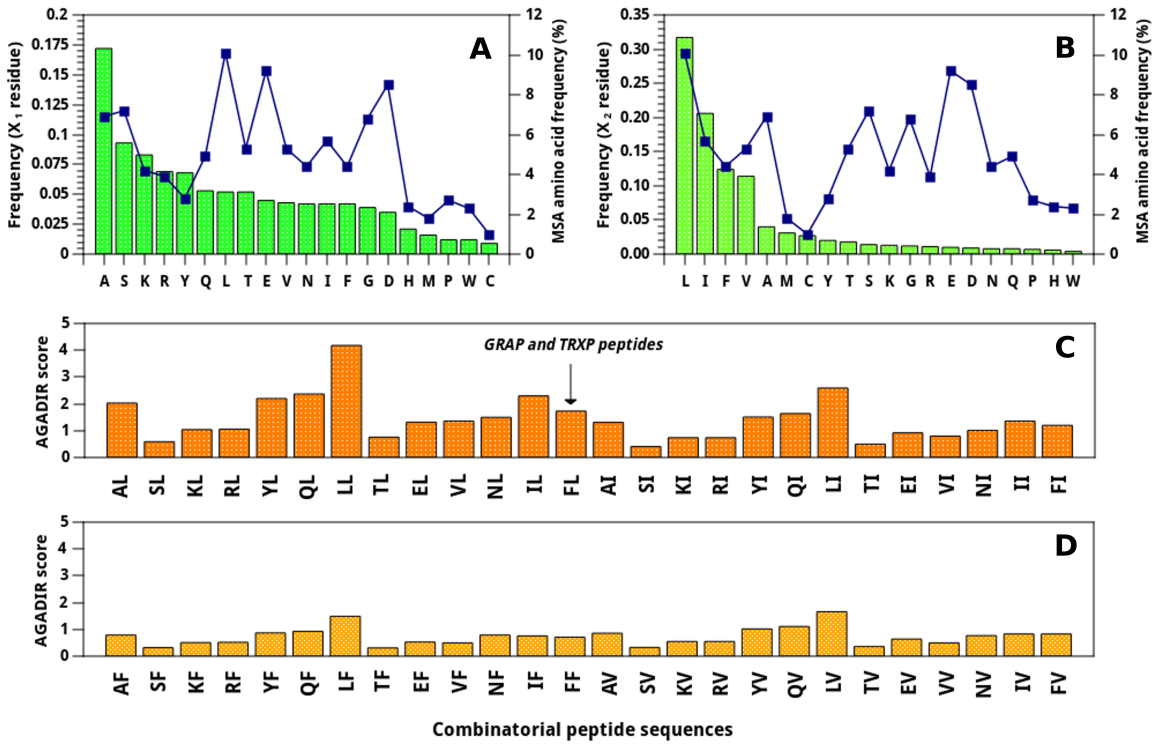

Figure S1. Sequence Analysis of the EExxED Motif: sequence conservation and secondary structure stability predictions by AGADIR for the contribution of residues xx. The frequency (green bars) at which each amino acid residue is located in positions 22 (x_1) and 23 (x_2) in the global alignment is shown in (A) and (B), respectively. In addition, the frequency of occurrence of each amino acid residue in any position of the alignment is shown (blue squares, as a percentage) to take into account bias in the sequence family. Secondary structure stability prediction was carried out using AGADIR for each member of a family of peptides in which x_1 and x_2 emerge as the combination of the more frequently occurring amino acids for each position using a cut off of 73% and 76% for x_1 and x_2, respectively.

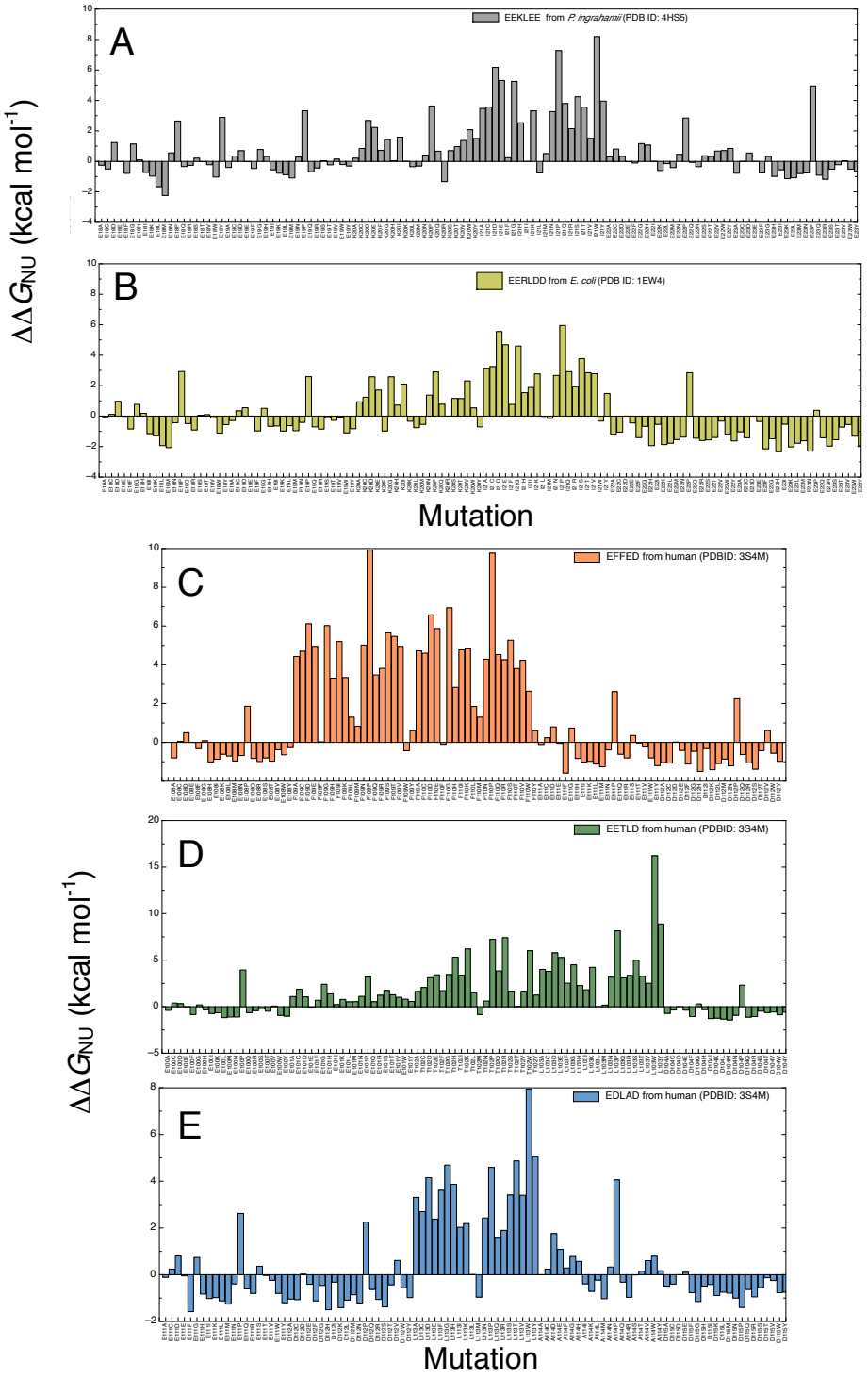

Figure S2. Analysis of the EExxED Acidic Mtif: Predictions of the Contribution of Residues xx to the Global Stability by FOLDX. The contribution of each position in the

acidic motif to the total difference in free energy of between folded and unfolded states of FXN variants calculated using FOLDX algorithm. (A) and (B) Sequences EEKIEE and EERLDD from *P. ingrahamii* (residues 18-22, PDB ID: 4HS5) and *E. coli* respectively (residues 18-22, PDB ID: 1EW4) FXN proteins. (C), (D) and (E), the human FXN (PDBID: 3S4M, helix–α1) sequences EFFED, EETLD, and EDLAD, respectively. Each residue of the motif was mutated for each one of the 20 amino acid residues. Then the structure was repaired using the tool repair and the energy (and the difference in energy between the wild type and the mutant was calculated. Positive and negative values indicate mutations that destabilize or stabilize the structure of the native state, respectively.

In human FXN (PDBID: 3S4M and 1EKG) a partial motif of acidic residues is repeated three times in the helix–α1 context: (i) EETLD (residues 100-104), in which –OH group of T102 interacts with the indole nitrogen of Trp173 (forming an hydrogen bond) and L103 establishes core interactions; (ii) EFFED (residues 108-112), in which Phe residues establishes interactions with helix α2, as well as the C-terminal region of FXN and with the β–sheet; and (iii) EDLAD (residues 111–115), in which the L113 is located in an apolar environment contributing to the stability of the protein, whereas A114 is situated in a partial solvent-exposed position. In this case, a partial shift in register of the acidic side chains on the helix may take place, but the shift is rather limited because acidic residues must be full exposed to the solvent, and packing of the helix with the rest of the protein must be guaranteed. Similarly, for *P. ingrahamii* (PDB ID: 4HS5) and *E. coli* (PDB ID: 1EW4) variants, the sequence EEKIEE (residues 18–22) and EERLDD (residues 18–22) charged groups of the K20 and R20 are partially exposed to the solvent (interestingly, R20

is interacting with W88 through a π–cation interaction), whereas residues I21 and L21 interact with the core of each protein variant.

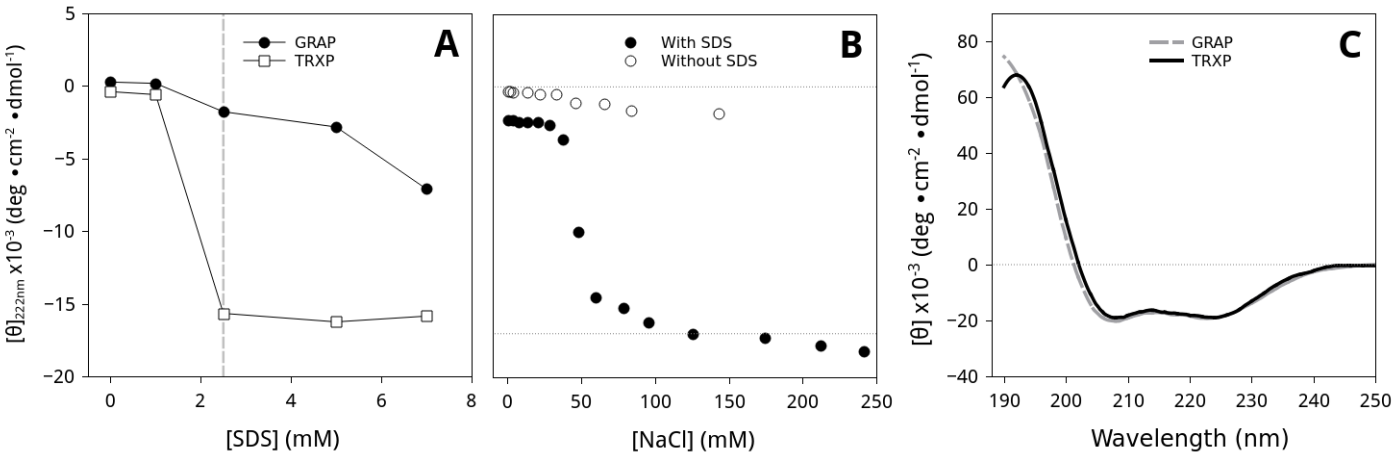

Figure S3. α-Helical Propensity of GRAP and TRXP. (A) Induction of α–helical by SDS of GRAP (•) and TRXP (□) followed by CD at 222 nm. Buffer was 10 mM Tris–HCl, pH 7.0. (B) Induction of α-helical of GRAP (•) by the addition of NaCl in buffer 20 mM Tris–HCl, 2.5mM SDS, pH 7.0. As a control sample, the GRAP peptide was diluted with the same buffer without NaCl. (C) Far-UV CD spectra corresponding to GRAP (gray dashed line) and TRXP (black solid line) in the presence of 25% TFE. Experiments were performed at 25 °C.

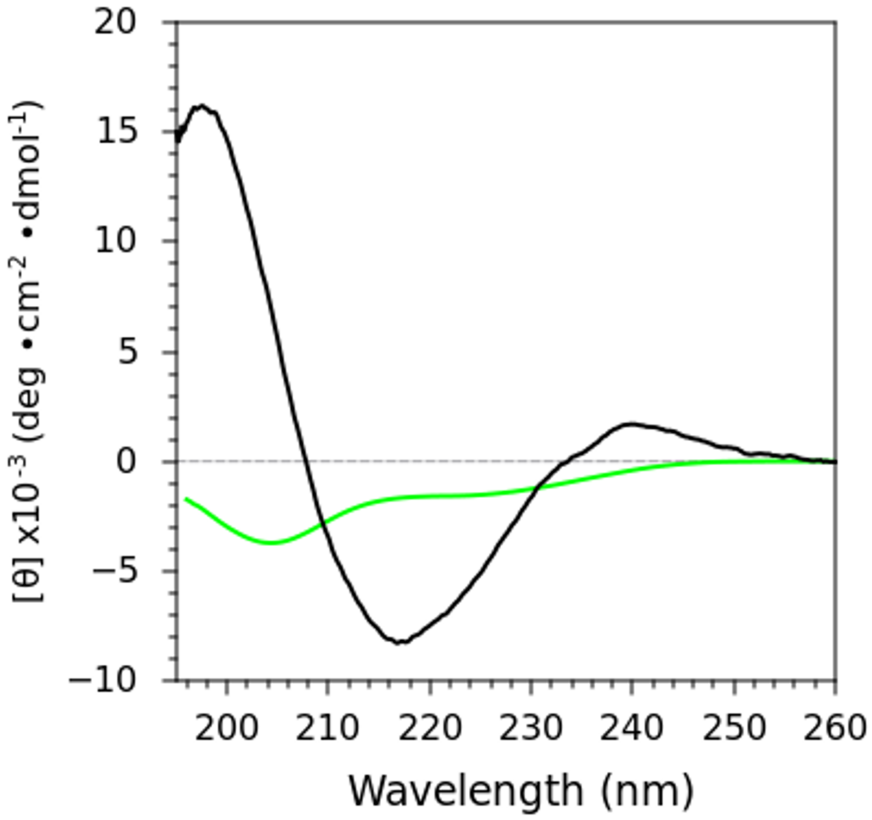

Figure S4. Far-UV CD spectra corresponding to GRAP in the presence of 300 μM $PdCl_2$ or in the absence of the metal ion are shown in black solid and green dashed lines, respectively. Buffer was 20 mM sodium acetate, pH 4.1 and peptide concentration was 25 μM. A 10–min incubation and the experiment were both carried out at 25 °C.

Capillary Zone Electrophoresis Results

As the net charge of GRAP must change after Fe^{+3} binding, we used capillary zone electrophoresis (CZE) to investigate changes in mobility (migration time) due to the complex formation. Figure S3 shows the CZE profiles for both peptides, in the absence (Figures S3A and B) or the presence of Fe^{3+} (**Figures S3C** and **D**). It is worthy of note that the elution profiles of both peptides exhibit a certain heterogeneity as inferred from the number of peaks, more likely due to the presence of different conformations in solution.

In the absence of the metal ion, GRAP exhibited longer elution times according to its larger negative charge, by comparison with the peptide TRXP. On the contrary, when iron was added to GRAP, the migration time corresponding to a significant fraction of peptide was similar to that observed for TRXP. These results indicate that most probably, the iron–GRAP complex is less negative-charged than the isolated GRAP. On the other hand, the addition of iron to TRXP did not significantly alter its behavior, suggesting no interaction of the metal ion with this peptide under these experimental conditions, in agreement with the CD results.

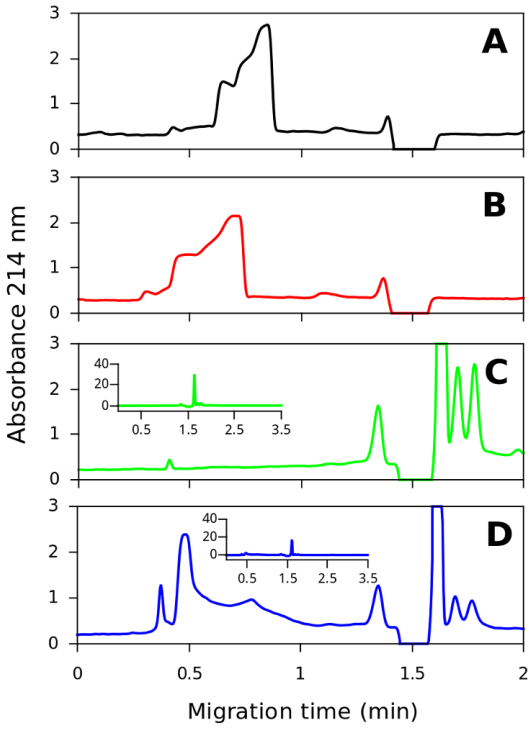

Figure S5. Capillary Zone Electrophoresis of Peptides. Samples of TRXP (A and B) and GRAP (C and D) were prepared without (A and C) or by the addition of an equimolar Fe^{3+} concentration (B and D). In all cases, peptide concentration was 100 μM and buffer was 20 mM potassium acetate, pH 4.1. No iron was added to the running buffer. All experiments were carried out at 25 °C. The TRXP sample was run as a control. The insets in C and D show the zoom out of each profile.

Iron Parametrization and Conformational Search Using Autodock

To evaluate the molecular details concerning iron binding, we performed molecular dynamics simulations. For this purpose, a set of Lennard–Jones parameters for Fe^{3+} were set: R_{min} = 0.7 Å and ε = 1 kcal mol^{-1}, **Figure S4** and **Table S1**. Afterwards, conformational searches on the iron-peptide complex were carried out using the Autodock4.2 package [1] with the peptide backbone restricted to α-helix conformation. Only bi- and tridentated geometries were obtained for the Fe^{3+}–GRAP complexes (**Table S2**). Notably, the conformational search results showed that for tridentated complexes, residues D12 and E7 do not simultaneously participate in metal binding because they are far away in the α-helical context. Consequently, two different tridentated complexes were defined: *complex 1* (**Figure S5A**), where GRAP directly interacts with iron via E7, E8 and E11; and *complex 2* (**Figure S5B**), interacting via E8, E11 and D12.

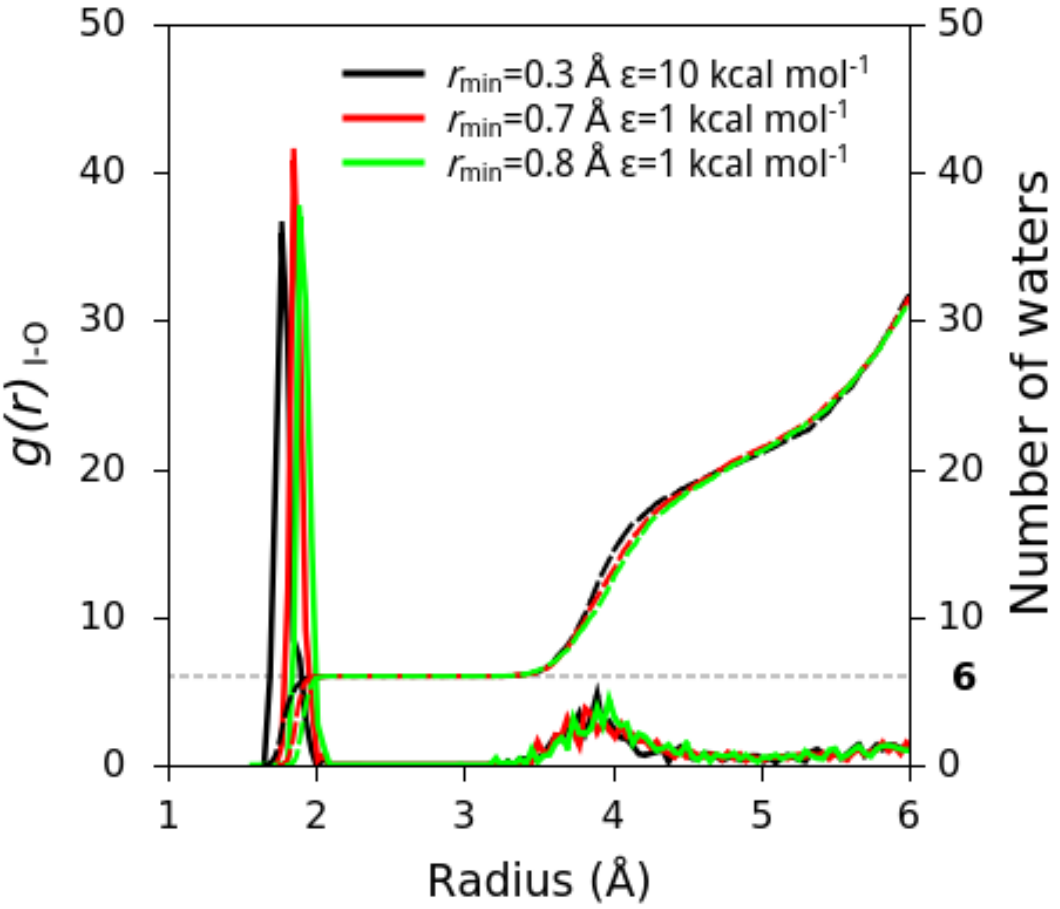

Figure S6. Radial Distribution Functions for Water–Iron Interaction. Relative water density as a function of the distance from the center of the metal ion (solid lines–left axis) and the number of water molecules at each radius (dashed lines – right axis) are shown.

Table S1. Parameters for Fe^{3+} metal ion simulations using a metal-water system and performing thermodynamic integration on MDs.

LJ Parameters (r_{min}; ε)	**ΔHFE[1] (Kcal/mol)**	**ΔIOD[2] (Å)**
0.3 ; 10	-41.04	-0.24
0.7 ; 1	-90.01	-0.14
0.8 ; 1	-117.02	-0.09

[1] The difference between the calculated and experimental values of hydration free energy (HFE).

[2] The difference between the calculated and experimental values of the ion-oxygen distance (IOD).

The Lennard–Jones parameter for the metal was varied, whereas the charge was set at +3. The IOD, the coordination number, and the water residence time were all determined by radial distribution function analysis. Experimental values of the HFE and IOD are 1018.68 kcal mol^{-1} and 2.00 Å. [2]

Table S2. Screening Cycle Results of Autodock Evaluation

Number of Evaluations	**complex (%)**				**Average Free Binding Energy (kcal/mol)**			
(ga_num_eval)	**mono**	**bi**	**tri**	**tetra**	**Bi**	**+/-**	**tri**	**+/-**
50	0	0.28	0.72	0	-13.16	0.38	-15.43	1.10
75	0	0.24	0.76	0	-13.18	0.41	-15.51	1.07
100	0	0.25	0.75	0	-13.03	0.43	-15.43	1.03
125	0	0.23	0.76	0	-13.03	0.43	-15.42	1.11
150	0	0.22	0.77	0	-12.99	0.48	-15.47	1.11
200	0	0.24	0.76	0	-12.96	0.56	-15.47	1.13
250	0	0.22	0.77	0	-12.98	0.61	-15.48	1.15
300	0	0.22	0.78	0	-13.01	0.60	-15.46	1.15
350	0	0.22	0.78	0	-12.98	0.66	-15.45	1.14
400	0	0.22	0.77	0	-12.98	0.64	-15.45	1.16
500	0	0.22	0.77	0	-13.00	0.64	-15.43	1.15
600	0	0.22	0.77	0	-12.96	0.67	-15.45	1.14
700	0	0.23	0.77	0	-12.97	0.68	-15.46	1.12
800	0	0.23	0.77	0	-12.93	0.68	-15.47	1.12

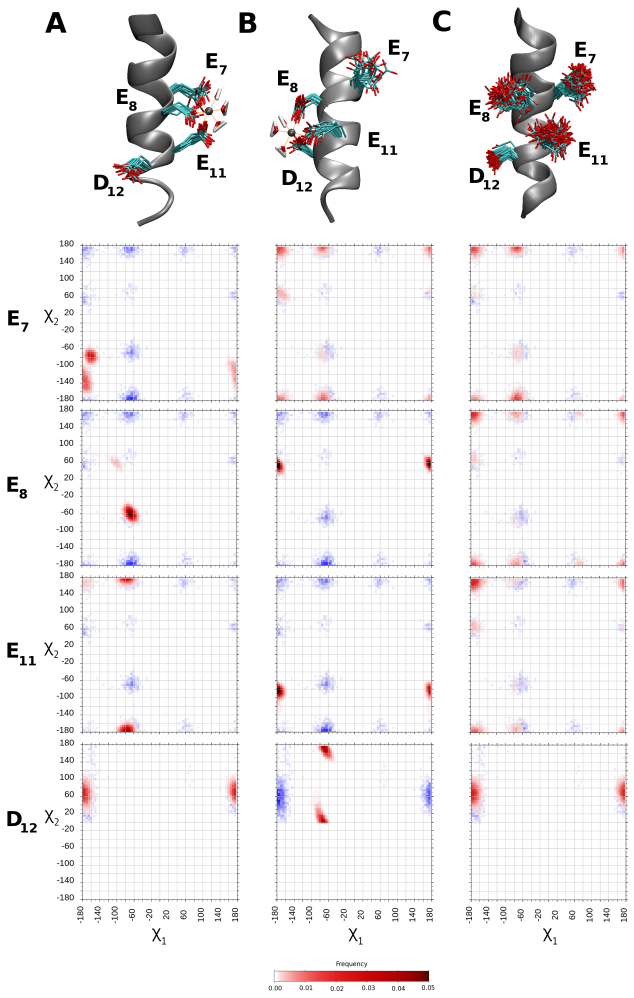

Figure S7. Side–chain Rotamers Populated along the MDs of Complex 1 (A), Complex 2 (B) and Free GRAP (C). In all cases, the backbone was restricted to the α-helical conformation. In each panel, the rotameric population corresponding to free Asp or Glu is shown in blue as a reference.

All-atom Restrained Molecular Dynamics Simulations

To accurately sample the conformation of GRAP side chains in the context of the iron-peptide complex in α–helical conformation, all-atom restrained molecular dynamics simulations (MDs) were performed. Only tridentated complexes where taken into account because they were reported as the *lower binding free energy* structures, by comparison with bidentated ones using the output Autodock (**Table S2**). The analysis of the MDs shows a change in the distribution of side-chain rotameric populations in the presence of Fe^{3+} (**Figure S5**, lower left and central panels). Residue E7 of *complex 1* acquired a conformation that is very low populated in the case of metal-free GRAP. Similar results were obtained for E11 and D12 of *complex 2* (Figure S5, lower right panels). Noteworthy are the computational results showing that GRAP in α-helical conformation may properly interact with Fe^{3+} in the region of the iron–binding motif by a local adjustment of the side–chain rotamers.

Table S3. Rotamer percentage for acidic residues in proteins (α–helical context) and MDs of complexes.

	Lovell *et al*. database [3]		
	Glu		Asp
	χ_1 (%)	χ_2 (%)	χ_1 (%)
[1]p	1	11	2
[1]t	36	62	19
[1]m	56	20	77
Total	93	93	98

	Complex 1		Complex 2	
	GLU 7			
	χ_1 (%)	χ_2 (%)	χ_1 (%)	χ_2 (%)
P	-	-	1.92	13.16
T	100	34.80	59.71	80.76
M	-	65.20	38.37	6.08
Total	100	100	100	100
	GLU 8			
P	-	8.27	-	99.97
T	0.84	-	99.97	-
M	99.16	91.73	0.03	0.03
Total	100	100	100	100
	GLU 11			
P	1.19	0.01	-	-
T	9.24	99.99	100.00	1.83
M	89.56	-	-	98.17
Total	100	100	100	100
	ASP 12			
P	-	95.55	-	
T	99.93	0.45	-	
M	0.07	-	100.00	
Total	100	100	100	

[1] p, t and m correspond to plus ($0°<\chi_1<120°$), trans ($120°<\chi_1<270°$) and minus ($270°<\chi_1<360°$), respectively.

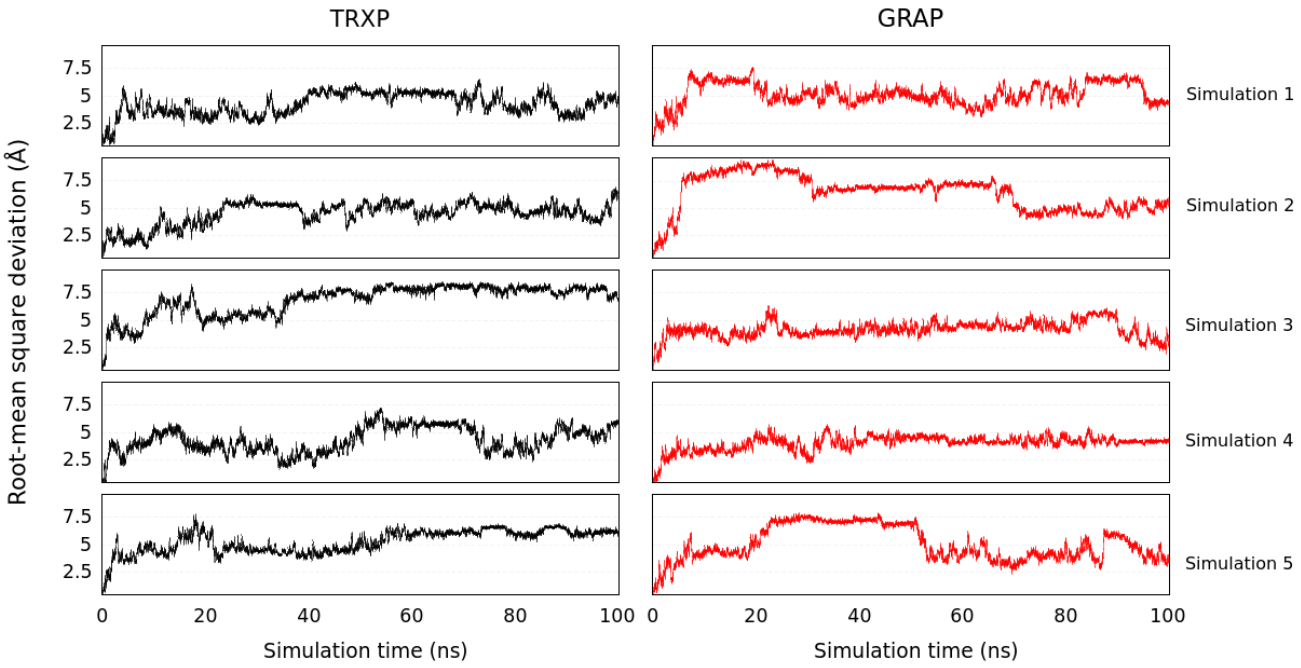

Figure S8. Molecular Dynamics Simulations**.** Five runs of 100 ns of each peptide TRXP, (black) and GRAP (red) were carried out in the absence of Fe^{3+} as control MDs. The RMSD value (Å) along the simulations is plotted as a function of the simulation time using the starting α–helical conformation as the reference structure.

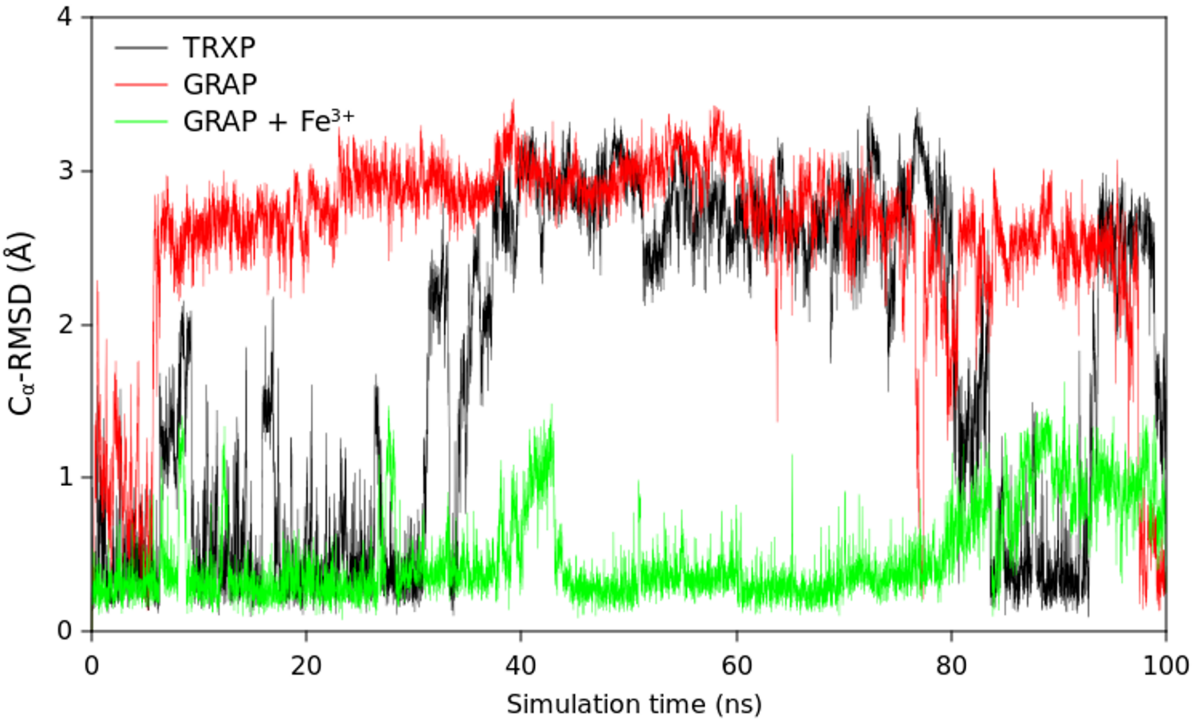

Figure S9. The RMSD of alpha carbon atoms corresponding to the residues EEFLED of GRAP (red) and iron–GRAP complex (green) are shown. The iron–binding motif of the iron-GRAP complex keeps its conformation throughout the simulations. In addition, the RMSD corresponding to the KEFLD residues of TRXP is shown as a control (black).

pKa Values of the Acidic Side Chains Calculated by Classical Thermodynamic Integration

Changes in the pH may alter these results since it may modify the total charge of the binding site and the repulsion between the anionic side chains previous to binding. It is noteworthy that p*K*a values of the acidic residues clustered in the motif can be considerably higher than the ones expected for isolated Glu or Asp residues. As the protonation state of acidic side-chain residues of the motif may be anomalous due to the negative-charged environment, we calculated the p*K*a shift corresponding to each acidic side chain of GRAP by classical thermodynamic integration using the linear mixing soft-core scaling method on the unbounded restricted system.[4] Twelve lambda values were used according to a Gaussian quadrature, and for each lambda, 2 ns were simulated on the NPT ensemble. Each pK_a value was obtained adding the calculated shift to the corresponding experimental value for the free amino acid side chain in solution. The result (**Table S3**) suggests that at least one of the four acidic side chains involved in the putative Fe binding motif might be protoned at pH 7.0. This may be particularly relevant in the context of FXN, where a number of iron–binding sites like this are present along the helix α1.

Table S4. The p*K*a values corresponding to each acidic side chain of GRAP calculated by classical thermodynamic integration MD.

Residue	pKa value
Glu 7	6.3
Glu 8	9.5
Glu 11	6.9
Asp 12	8.6
[1]Glu (free)	4.4
[1]Asp (free)	3.9

[1] The reference p*K*a value for the free amino acid in solution (side–chain).

Thermodynamic Integratios: Specificity of the Acidic Residue Motif for Iron Binding

We performed TI[4-6] for Fe^{2+}, Mg^{2+}, Co^{2+}, Mn^{2+} and Ca^{2+} metal ions (implemented in Amber14). **Table S5** contains a summary of these results suggesting that there is an energy gap between the binding of Fe^{2+} to GRAP and the other metal ions. However, solvation energies of the metal ions determined by TI, which represent for us a quality control, are not coincident with the experimental values (**Table S5**), even when the radial distribution functions (metal: oxygen) are coincident with the expected ones (**Table S5**). Thus, in this case, there is no guaranty that parameters, which correctly reproduce solvation geometries (and solvation energies in the best scenario), describe the energetics of metal:peptide interactions.

Table S5. Thermodynamic Integration and Specificity of the Acidic Residue Motif for Iron Binding.

Metal Ion	**Metal-Oxygen Distance[1] (Å)** Amber14 (experimental)	**ΔG° solvation (kcal mol^{-1})** Experimental	**ΔG° solvation[3] (kcal mol^{-1})** Amber14	Metal:peptide **ΔΔG° Binding[4] (kcal mol^{-1})** Amber14
Fe^{2+}	2.12 (2.12)[2]	-451.8	-452.72	---
Co^{2+}	2.08 (2.08)	-481.0	-517.86	-3.4
Mg^{2+}	2.10 (2.10)	-454.2	-457.16	6.15
Mn^{2+}	2.2 (2.2)	-436.4	-426.88	3.13
Ca^{2+}	2.39 (2.39-2.46)	-379.5	-348.62	18.23

[1]Metal-oxygen distances (metal to H_20) were taken from the peak of the radial distribution functions.
[2] Experimental values for metal-oxygen (H_2O) distance are shown in brackets.
[3] Free energies of solvation calculated from simulations applying thermodynamic integration procedures as indicated under Materials and Methods, below.
[4]The free energy differences of binding were calculated taking Fe^{2+} as the reference as indicated applying thermodynamic integration procedures (**Equation 3**).

Methods used for TI/ MDs that we carried out.

To characterise the binding process in terms of its energetics and specificity, we carried out classical thermodynamic integrations (TI) for the 2+ series of metal ions: Fe^{2+}, Mg^{2+}, Co^{2+}, Mn^{2+} and Ca^{2}. For that, we used metal ion parameters obtained by Duarte *et al.*[7] Parameters were transferred to Amber14. First we considered the following processes:

$GRAP{:}\,Fe^{2+}(aq) \rightarrow GRAP + Fe^{2+}$ (aq) (1)

$GRAP + M^{2+}(aq) \rightarrow \quad GRAP{:}\,M^{2+}$ (aq) (2)

$\mathrm{G}RAP{:}\,Fe^{2+}$(aq) $+ M^{2+}(aq) \rightarrow Fe^{2+}(aq) + GRAP{:}\,M^{2+}(aq)$ (3)

However, these processes include MD simulations of free peptide and metal dissociation, and both kinds of simulations would require very large simulation times. On the other hand, the processes described below have allowed us to calculate the difference in free energies when binding between two different metals with better accuracy. It is worthy of note that the sum of chemical **Equations 4** and **5** results in the chemical **Equation 3**.

$GRAP{:}\,Fe^{2+}(aq) \rightarrow GRAP{:}\,M^{2+}\ \ (aq)$ (4)

$M^{2+}(aq) \rightarrow Fe^{2+}\ (aq)$ (5)

Therefore, a peptide-metal ion complex in which GRAP coordinates Fe^{2+}through E7, E8 and E11 was prepared and unconstrained MD simulations were performed.

Parameters of Fe^{2+} were turned into those of each one of the other metal ions using the linear mixing potential scaling method on the system. Fifty one-lambda (λ) values were used, and for each lambda, 50 ps were simulated on the NPT ensemble. The first 5% of each simulation (equilibration) was not taken into account for the analysis. A mixing Hamiltonian $H_{(\lambda)}$ between the initial ($H_{(0)}$ and the final ($H_{(1)}$ states is used in the simulations. Each λ window of the TI started using the final snapshot of the previous window as the input structure. The Hamiltonian associated to each ensemble was expressed as:

$$H(p,q,\lambda) = H_o(p,q) + (1-\lambda)H_{\lambda=0(p,q)} + (\lambda)H_{\lambda=1(p,q)} \quad (6)$$

where p and q are vectors corresponding to generalised momentum and atomic positions, respectively and ΔG ($Fe^{2+} \rightarrow M^{2+}$) of replacement of Fe^{2+} by other metal M^{2+}

$$\Delta G = \int_0^1 \langle \partial G/\partial\lambda \rangle \partial\lambda = \int_0^1 \langle \partial V/\partial\lambda \rangle \partial\lambda \quad (7)$$

in which V is the potential energy and < > indicates the time average. Finally, derivative of $\partial V/\partial\lambda$ was integrated to obtain a free energy difference that represents the process described by **Equation 4**, where M is Mg^{2+}, Co^{2+}, $Ni^{2+,}$ Mn^{2+}, Ca^{2+}or Zn^{2+}.

The same procedure was carried out for free metal ions (solvated ions) obtaining the difference in free energy of the process described by chemical **Equation 5.** The difference in free energy corresponding to the binding process (the sum described by **Equation 3**) includes both free energy terms (**Equation 4 and Equation 5**).

To obtain free energies of solvation we simulated the removal of the metal ion from a water-filled simulation box. In these simulations, the initial state corresponded to the solvated metal ion and the end state to a box of pure water.

References

1. G. M. Morris, R. Huey, W. Lindstrom, M. F. Sanner, R. K. Belew, D. S. Goodsell and A. J. Olson, *J Comput Chem*, 2009, 30, 2785-2791.
2. H. Ohtaki and T. Radnai, *Chemical Reviews*, 1993, 93, 1157-1204.
3. S. C. Lovell, J. M. Word, J. S. Richardson and D. C. Richardson, *Proteins*, 2000, 40, 389-408.
4. T. Steinbrecher, D. L. Mobley and D. A. Case, *The Journal of chemical physics*, 2007, 127, 214108.
5. T. Steinbrecher, I. Joung and D. A. Case, *J Comput Chem*, 2011, 32, 3253-3263.
6. F. M. Ytreberg, R. H. Swendsen and D. M. Zuckerman, *The Journal of chemical physics*, 2006, 125, 184114.
7. F. Duarte, P. Bauer, A. Barrozo, B. A. Amrein, M. Purg, J. Aqvist and S. C. Kamerlin, *The journal of physical chemistry. B*, 2014, 118, 4351-4362.